Asian Journal of Chemistry; Vol. 37, No. 8 (2025), 2051-2058

ASIAN JOURNAL OF CHEMISTRY

https://doi.org/10.14233/ajchem.2025.34120

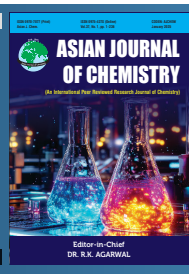

Fluorescent Schiff Base Chemosensor for Selective Detection of Cu^{2+} Ions, DFT Analysis and Anti-Alzheimer Potential

BHARAT BHUSHAN[1,*], ASIF JAMAL[2], MD. SERAJUL HAQUE FAIZI[2] and KAMAL RAJ SAPKOTA[3]

[1]Department of Chemistry, M.P.S. Science College (Affiliated to B.R.A Bihar University), Muzaffarpur-843165, India
[2]PG Department of Chemistry, L.S. College (Affiliated to B.R.A Bihar University), Muzaffarpur-842001, India
[3]Department of Chemistry, Tribhuvan University, Prithvi Narayan Campus, Pokhara, Nepal

*Corresponding author: E-mail: bbharat.uohy@gmail.com

Received: 25 May 2025; *Accepted*: 27 July 2025; *Published online*: 31 July 2025; AJC-22085

In this work, a Schiff base chemosensor (6-hydroxy-N′-(pyren-1-ylmethylene)-2-naphthohydrazide) (HL) was synthesized, which can be used for the detection of Cu^{2+}. This shows excellent selectivity towards Cu^{2+} ions at pH 7.4. The association constant (K_a) of the chemosensor for binding with Cu^{2+} was 1.16×10^4 M^{-1}. Using the Benesi–Hildebrand relation, the stoichiometric ratio for complexation was found to be 1:1. The DFT method, the B3LYP functional and the 6-311++G(d,p) basis set were employed to calculate the frontier molecular orbital (FMO) analysis and molecular electrostatic potential (MEP). Based on the docking investigation, the Schiff base exhibits the anti-Alzheimer capability when docked with the receptors AChE and BChE with a binding affinity of -14.6 kcal/mol and -12.7 kcal/mol, respectively. Druglike nature, medicinal chemistry friendliness, and multiple toxicological were predicted using free SwissADME software.

Keywords: Schiff base, Chemosensors, Hydroxy, Functional group, DFT method, Anti-Alzheimer activity.

INTRODUCTION

In recent years, the design and synthesis of fluorescent chemosensors have drawn a lot of attention from chemists as these are highly selective and sensitive to particular metal ions [1-4]. The organic chemosensors utilize the property of fluorescence and have tremendous applications in analytical and environmental chemistry [5,6]. Copper is the third most abundant metal in the human body and Cu^{2+} ions play an influential role as a catalytic cofactor for many metalloenzymes and other biological processes [7-9]. However, the excess amount of copper ion in the human body can lead to various diseases like Alzheimer's disease [9], Parkinson's disease [10], Wilson's disease [11] and amyotrophic lateral sclerosis [12]. The maximum acceptable concentration of Cu^{2+} ions in drinking water is 20 µM. Excessive amounts of copper in drinking water have resulted in Cu^{2+} ions as important pollutants in the environment. Therefore, the detection of Cu^{2+} ions is highly important for both the biological system and the environment. There are various kinds of literature available for spectroscopic methods of detection of such ions, like absorption spectroscopy, inductively coupled plasma optical emission spectrum, electrochemical methods, flame absorption spectroscopy, *etc.* [13-15]. However, these techniques have several disadvantages like high instrument cost, low sensitivity, complex processes, *etc.* Therefore, a strong need for cost-effective, highly sensitive, highly selective calorimetric sensors are required, which can detect these metal ions through fluorescence-based techniques without using any expensive instruments [16-20].

While designing a fluorescent chemosensor, many different kinds of signaling mechanisms are taken into consideration, for example, photo-induced electron/energy transfer (PET) [21], intermolecular charge transfer (ICT) [22], fluorescence resonance energy transfer (FRET) [23] and imine isomerization [24]. Moreorver, these fluorescent chemosensors are also very cost-effective and promising chemosensors for the detection of the metal ions [25-28]. It is convenient to design these fluorescent techniques using a Schiff base. They easily form complexes with the target metal ions, showing fluorescent activity. There is a lot of literature available on calorimetric sensors for the detection of Cu^{2+} ions [29-32], but these sensors showed very poor selectivity and low sensitivity over other metal ions.

Furthermore, neurodegenerative syndrome, typically resulting from increasing memory loss and cognitive decline in elderly person persons, is exemplified by Alzheimer's disease (AD). Inadequate concentration levels of acetylcholine in the brain are acknowledged to be a key contributing factor to AD. Inhibiting acetylcholinesterase (AChE) and butyrylcholine-sterase (BChE) is regarded as an influential therapeutic strategy for treating AD [33-36]. In this research work, a Schiff base fluorescent probe (6-hydroxy-N′-(pyren-1-ylmethylene)-2-naphthohydrazide) (**HL**) has been designed and synthesized. The sensor successfully detected the presence of Cu^{2+} ions in the real samples. Furthermore, FMO, DOS, MEP, ADMET and docking are also studied.

EXPERIMENTAL

All the chemicals including pyrene-1-carbaldehyde and 6-hydroxy-2-naphthohydrazide were obtained from Sigma-Aldrich Chemicals, USA and used without undergoing any additional purification. Spectroscopic grade solvents were obtained from Sigma-Aldrich Chemicals, USA and Sisco Research Laboratory (SRL) Pvt. Ltd., India. The metal ions solutions were prepared from either their perchlorate or nitrate salts. Analytical grade water was obtained from the Elix 10 water purification system. All experiments were performed at room temperature unless stated otherwise.

Characterization: IR spectra were recorded using Perkin-Elmer L 120-000A spectrometer with KBr pellets ranging from 4000-400 cm^{-1}. ^1H and ^{13}C NMR spectra were observed through Bruker DPX-400 MHz spectrometer. The chemical shift was reported as ppm taking $CDCl_3$, in which tetramethylsilane was taken as standard. Elemental analysis was carried out using PE2400 elemental analyzer. Fluorescence spectra were recorded using a Perkin-Elmer LS 45 spectrofluorometer. Steady-state absorption spectra were recorded on the Shimadzu UV-1601PC absorption spectrophotometer. Absorption and fluorescence spectra were scanned using Quartz cuvettes of 10 mm optical path length, which was obtained from Perkin-Elmer, USA (part no. B0831009) and Hellma, Germany (type 111-QS), respectively. For fluorescence emission and excitation spectra measurements, a 5 nm bandpass was used on the excitation and emission side.

Synthesis of 6-hydroxy-*N′*-(pyren-1-ylmethylene)-2-naphthohydrazide (HL): Pyrene-1-carbaldehyde and 6-hydroxy-2-naphthohydrazide in equal molar ratio (1.0 mmol) were mixed in ethanol solution (21 mL) and then refluxed for 10 h, which resulted in the formation of precipitate. The precipitate formed was filtered and recrystallized in 1:1 mixture of THF and ethanol (**Scheme-I**). Bright yellow crystals, yield: 90%. IR (KBr, ν_{max}, cm^{-1}): 3457, 3395, 3248, 1644, 1531, 1217. ^1H NMR (DMSO-d_6, 400 MHz) δ ppm: 12.21 (s, 1H, NH), 11.28 (s, 1H, OH), 9.49 (s, 1H, N=C-H), 8.88 (d, 1H, *J* = 8 Hz, Ar-H), 8.57 (d, 1H, *J* = 8 Hz, Ar-H), 8.55 (d, 1H, *J* = 16 Hz, Ar-H), 8.42-8.40 (m, 4H, Ar-H), 8.29-8.23 (q, 2H, Ar-H), 8.16 (t, 1H, *J* = 8 Hz, Ar-H), 7.89 (d, 1H, *J* = 8 Hz, Ar-H), 7.79 (d, 1H, *J* = 8 Hz, Ar-H), 7.75 (t, 1H, *J* = 8 Hz Ar-H), 7.49-7.54 (m, 2H, Ar-H); ^{13}C NMR (DMSO-d_6, 100 MHz) δ ppm: 163.60, 153.99, 147.19, 135.77, 131.93, 130.71, 130.23, 130.01, 128.67, 128.53, 128.37, 128.13, 127.27, 126.71, 126.49, 126.01, 125.73, 125.68, 125.11, 124.01, 123.70, 123.62, 123.06, 122.48, 120.18, 110.51. Elemental anal of $C_{28}H_{18}N_2O_2$ (*m.w.* 414.44), cald. (found) %: C, 81.20 (81.16); H, 4.45 (4.41); N, 6.81 (6.73).

Computational details: The synthesized HL's frontier molecular orbitals (FMO) and molecular electrostatic potential (MEP) were examined using the Gaussian 09 software package [37]. These computations were carried out using the density functional theory (DFT), explicitly applying the B3LYP and 6-311++G(d,p) functional and basis set.

Docking and ADMET: The molecular docking examination of HL with protein AChE and BChE has been executed by AutoDock Vina and Auto Dock tool [38]. The online server Swiss ADME (http://www.swissadme.ch/index.php) was employed to achieve the ADMET investigation for HL.

Docking analysis: In this study, the fluorescent Schiff base (HL) was docked with the active sites of the receptors AChE and BChE to investigate the binding capacity for developing HL as a probable therapeutic candidate for Alzheimer's disease treatment. The AChE (PDB ID-1EVE) and BChE (PDB ID-1P0I) receptors have been obtained from the protein data bank (PDB) in PDB file format and opened in Discovery Studio. The receptors were then prepared for docking. During preparation, the water molecules were first removed, polar hydrogens were added and Gasteiger charges were assigned [35,39,40]. Finally, the receptor and ligand were converted into PDBQT format and docked using AutoDock Vina. The grid was configured with dimensions of 20 × 20 × 20 $Å^3$ along the x, y and z axes. For HMDP-AChE, the center was positioned at coordinates 21.226929, 62.206393 and 30.430250, while for HL-BChE, the center was set at 136.523857, 149.915929 and 26.730500 along their respective axes.

RESULTS AND DISCUSSION

A new fluorescent Schiff base (HL) were synthesized by condensing pyrene-1-carbaldehyde and 6-hydroxy-2-naphthohydrazide in ethanolic solution resulted in formation of the Schiff base fluorescent compound HL in 90% yield.

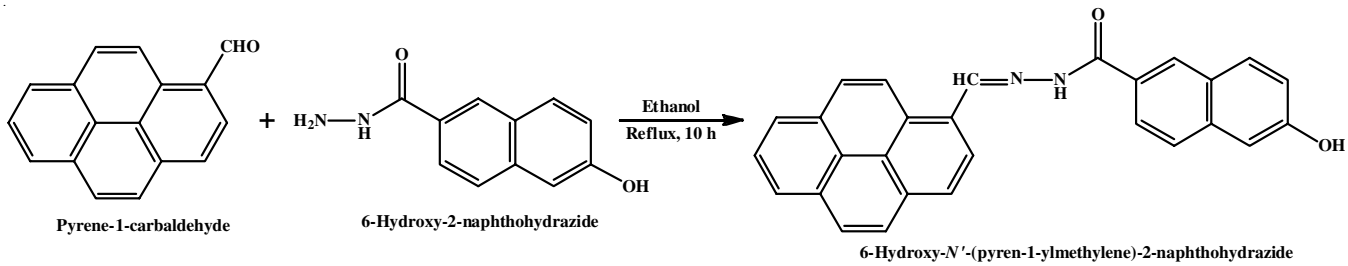

Scheme-I: Synthesis of chemosensor HL

Absorption and emission investigation: The UV-Vis spectrum of HL show an absorption peak at 393 nm, which is an intermolecular charge transfer transition. The HL (4×10^{-6} M) was mixed with 1:1 v/v solution of DMSO and water, HEPES buffer: 50 mM, pH 7, gave an emission band at 463 nm. On addition of Cu^{2+} ions, the fluorescent intensity was increased by four times. Under same conditions, when HL was treated with different metal ions like Pb^{2+}, Cd^{2+}, Zn^{2+}, Mg^{2+}, Ba^{2+}, Bi^{2+}, Hg^{2+}, Fe^{3+}, Ce^{3+}, La^{3+}, K^{+}, Ni^{2+}, Ca^{2+}, Zr^{2}, Mn^{2+}, Na^{+}, Ag^{+}, Co^{2+}, Li^{+}, Th^{4+}, Fe^{2+}, Al^{3+} and Sr^{2+} did not exhibit any substantial changes in the intensity of the emission spectra (Fig. 1). This suggests that the chemosensor HL binds effectively with Cu^{2+} ions, resulting in enhancement of the fluorescent intensity. Moreover upon excitation at 393 nm, the emission band increased to 467 nm with a small red shift as shown in Fig. 2.

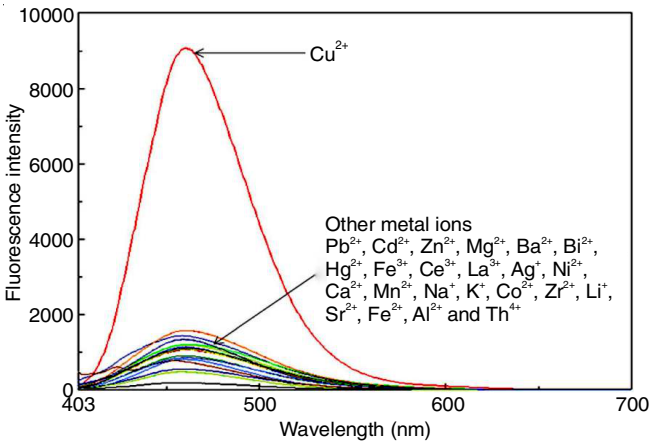

Fig. 1. Fluorescence spectra of chemosensor HL (4×10^{-6} M) with different metal ions

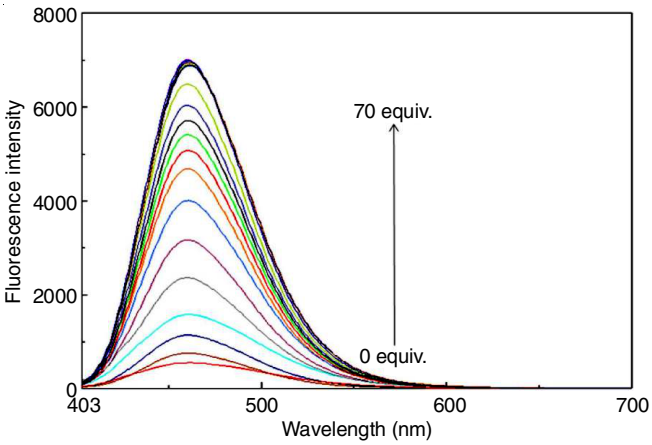

Fig. 2. Fluorescence spectra of chemosensor HL (4×10^{-6} M) with 0-70 equiv. of Cu^{2+}

Further, the competitive interference of the chemosensor for Cu^{2+} with other metal ions was monitored by mixing 100 equivalents of Cu^{2+} and 100 equivalents of different metal ions. From the competitive studies, it was observed that the fluorescent intensity of Cu^{2+} ions didn't alter with the addition of other metal ions (Fig. 3). This confirmed that the chemosensor HL could be employed to detect Cu^{2+} ions in real as well as biological samples.

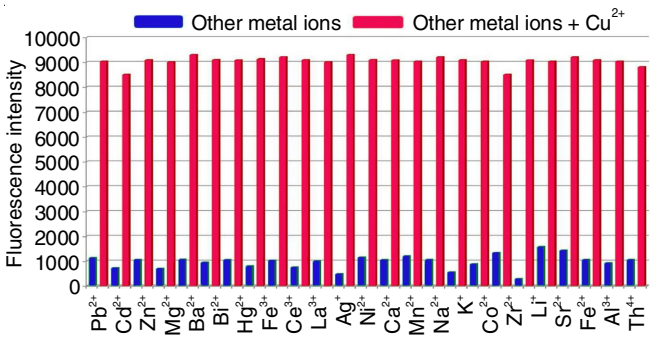

Fig. 3. Fluorescence spectra of chemosensor HL (4×10^{-6} M) with 100 equiv. of Cu^{2+} in presence (100 equiv.) and absence of other metal ions

Reversibility study of HL towards Cu^{2+} with Na_2EDTA: The reversibility study of the chemosensor HL towards Cu^{2+} was examined using EDTA titration. Fluorescence intensity was enhanced on the addition of Cu^{2+} ions (100 equiv.) to chemosensor HL. However, the fluorescence emission was quenched to the intensity of the original chemosensor HL by the addition of Na_2EDTA (100 equiv.). The cycle was repeated several times, which infers that the binding of Cu^{2+} with the chemosensor HL is in a reversible manner (Fig. 4).

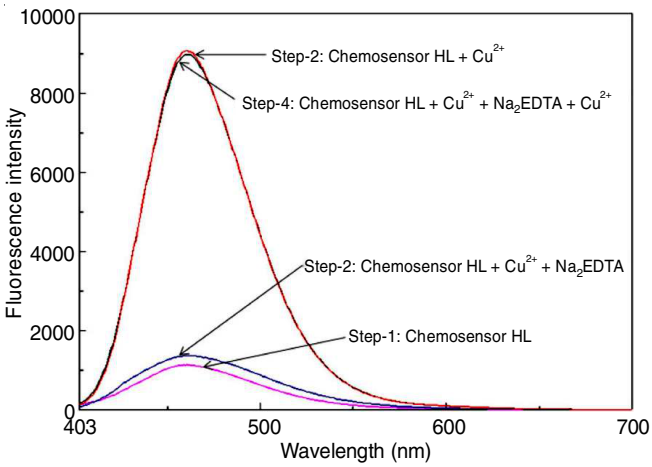

Fig. 4. Fluorescence spectra of chemosensor HL (4×10^{-6} M) in presence of Cu^{2+} and Na_2EDTA

Effect of pH and time dependence studies: The time-dependence fluorescence study was done on chemosensor HL in the presence of Cu^{2+} ions. Chemosensor and Cu^{2+} ions were mixed in 1:1 v/v DMSO-H_2O solution with 50 mM HEPES, pH 7.5. Results suggest that the binding time of Cu^{2+} ions with the chemosensor was 5 min. Hence, this time limit was set for all further fluorescence studies on this chemosensor. Further, the influence of pH on fluorescence intensity was examined. The pH range from 1-12 was investigated using 100 equivalents of chemosensor HL and 100 equivalents of Cu^{2+} ions. The result shows that free chemosensor HL does not show any significant change in its intensity; however, in the binding state with Cu^{2+} ions, the fluorescence intensity remains stable at 463 nm in the pH range from 5-9. Based on these studies, the optimum pH of 7.5 was selected for all further fluorescence studies (Fig. 5).

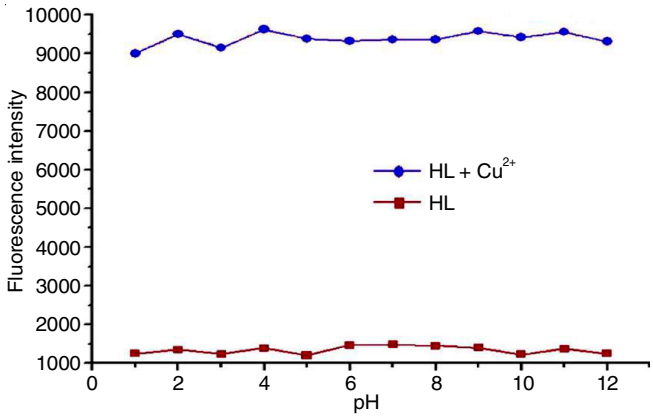

Fig. 5. Fluorescence response of chemosensor HL (100 equiv.) and after addition of Cu^{2+} (100 equiv.) at different pH

Stoichiometry of complexation: The Stoichiometric ratio of the HL:Cu^{2+} complex was determined utilizing Job's plot investigation. The interaction shows that at 463 nm, the maximum mole fraction of chemosensor HL was 0.5, which clearly suggests that the stoichiometry of complexation of the chemosensor and Cu^{2+} ion was 1:1 (Fig. 6a). This stoichiometry was further confirmed using Benesi- Hildebrand nonlinear curve fitting analysis. On analyzing the emission intensity data, the association constant of HL---Cu^{2+} complex was found out to be 1.16×10^4 M^{-1} (Fig. 6b). This data also suggests the complexation ratio of HL and Cu^{2+} complex to be 1:1. Further detection limit of the chemosensor was determined using titration method, which was found out to be 0.25×10^{-6} M.

FMO analysis: The investigation of frontier molecular orbitals (FMOs) provides a robust framework for analyzing the electrical and optical properties of materials. A key parameter in this investigation is the energy gap ($E_g = E_{LUMO}–E_{HOMO}$), which provides vital insights into the efficiency and performance of photovoltaic materials [41]. HOMO and LUMO are collectively acknowledged as FMO; HOMO is associated with the electron-donating capacity of the molecule, whereas LUMO indicates the electron-accepting capability of the molecule [33,34]. Further, the electron-donating ability of a molecule is associated with the HOMO, making the HOMO energy directly related to the ionization potential. Conversely, the LUMO, having vacant space to accept electrons, is associated with electron affinity [33,35,42]. The energies of HOMO and LUMO, along with the HOMO-LUMO gap, are crucial for determining global reactivity parameters. These include ionization potential (IP), nucleofugality (ΔE_n), fermi energy (E_f), electron affinity (EA), electronegativity (χ), hardness (η), electrophilicity index (ω), nucleophilicity index (ν), electrofugality (ΔE_e), chemical potential (μ), softness (s), optical frequency (ω_{op}), maximum charge transfer (ΔN_{max}), optical softness (σ_0), energy change (ΔE) and reflectivity (R) [33]. The parameters as described elsewhere [33,35,43] were calculated and their values are presented in Table-1. The sketched representations of the HOMO, LUMO and HOMO-LUMO gap plots in the gaseous phase are shown in Fig. 7. The calculated energy of the HOMO is -5.639 eV, corresponding to molecular orbital number 108 out of a total of 327 molecular orbitals. The energy of the LUMO is -2.090 eV, associated with molecular orbital number 109. Consequently, the HOMO-LUMO energy gap of the molecule (HL) is found to be 3.549 eV. Furthermore, The Gauss-Sum 3.0 [44] software was employed to generate the density of states (DOS) plot (Fig. 8), which highlights the population analysis for each orbital and furnishes a specific sketch of the molecular orbital characteristics over a certain range of energy [42,45].

TABLE-1
COMPUTED VALUES OF GLOBAL REACTIVITY PARAMETERS (GRP)

GRP	Values	GRP	Values
IP (eV)	5.639	ΔE_n (eV)	-2.572
HOMO (eV)	-5.639	LUMO (eV)	-2.090
EA (eV)	2.090	ΔE_e (eV)	8.959
E_g (eV)	3.549	ω_{op} (eV)	6.294
μ (eV)	-3.864	χ (eV)	3.864
η (eV)	1.774	R (eV)	-0.127
s $(eV)^{-1}$	0.281	ΔE (eV)	–4.20
ω (eV)	4.206	ΔN_{max}	2.178
ν $(eV)^{-1}$	0.237	σ_o $(eV)^{-1}$	0.281
E_f (eV)	-3.865		

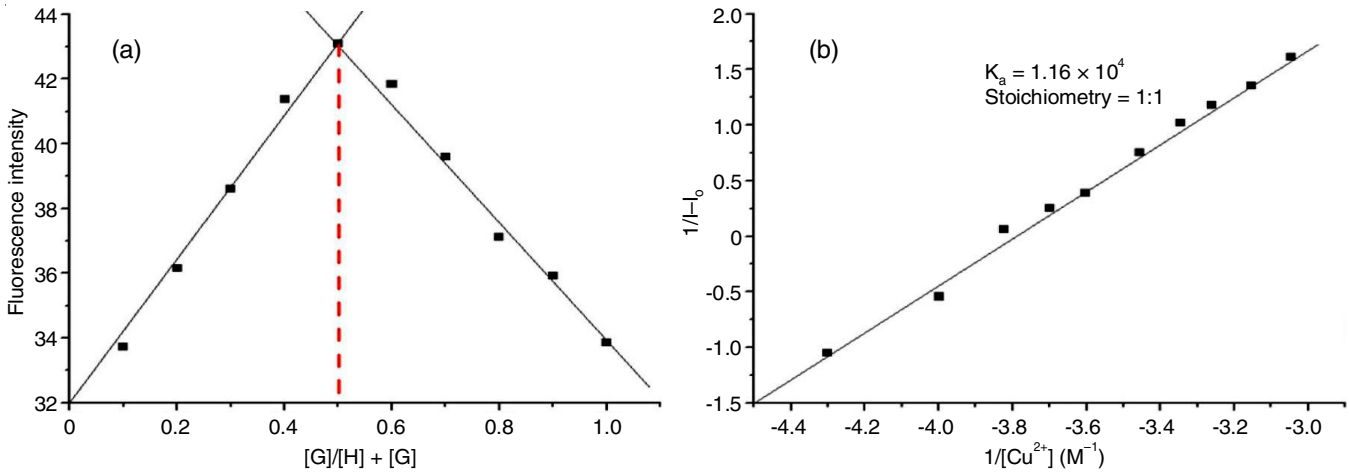

Fig. 6. (a) Job's plot and (b) Benesi-Hildebrand's plot of chemosensor HL with Cu^{2+} ion

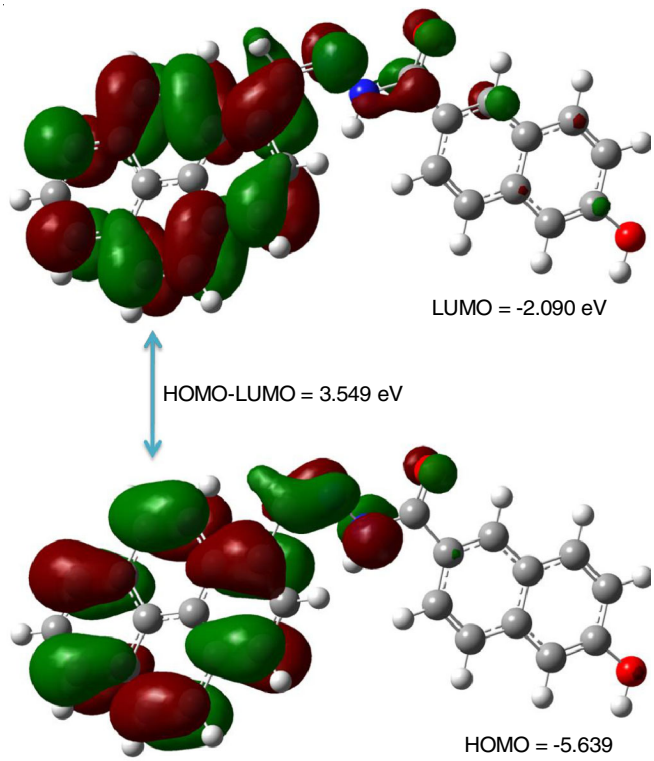

Fig. 7. The HOMO, LUMO and energy gap of synthesized Schiff base (HL)

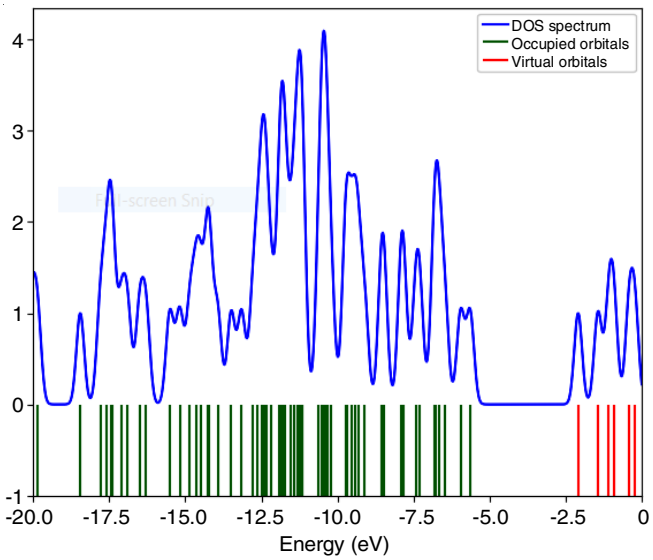

Fig. 8. Density of states (DoS) plot of synthesized Schiff base (HL)

The calculated IP and EA values are 5.639 eV and 2.090 eV, respectively. The maximum charge transfer is 2.178, indicating that the Schiff base compound has a tendency to react swifty and also demonstrates moderate stability [35,46,47]. The negative chemical potential value further confirms the chemical stability of compound. The calculated electrophilicity index is 4.206 eV, while the nucleophilicity index is 0.237, below 2.0 eV, classifying the title compound as a marginal nucleophile [35,46]. The computed hardness value is 1.774 eV and the energy change is –4.20 eV, suggesting the compound's capacity for electron transfer [35,48]. The softness and electronegativity values are found t obe 0.281 and 3.864 eV, respectively.

Molecular electrostatic potential (MEP): Fig. 9 shows the MEP map of HL, with a colour range spanning from -9.150e^2 to 9.150e^2. The negative areas, portrayed in red, are primarily associated with electron-rich functional groups such as imine, ketone and hydroxide groups, indicating areas of high nucleophilicity and potential sites for electrophilic attack. Contrarily, the positive regions, illustrated in blue, are concentrated around carbon and hydrogen atoms, signifying electron-deficient zones and potential sites for nucleophilic interactions. The MEP map highlights the compound's electronic characteristics, aiding in understanding its reactivity and interaction potential in molecular systems [33,35,46].

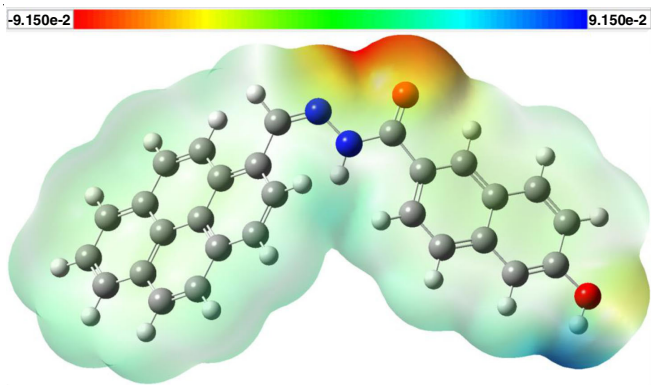

Fig. 9. MEP image of synthesized Schiff base (HL)

ADMET studies: Using the Swiss ADMET, drug-likeness of the newly designed compound HL has been studied and the associated parameters that have been computed are drug-likeness, lipophilicity, medicinal chemistry, water-solubility and pharmacokinetics [33,34]. This computation implies that HL fully complies with the Lipinski's rule of five, exhibiting zero violations. However, to satisfy the Lipinski's rules, a molecule would contain a molecular weight (MW) less than or equal to 500 g/mol, TPSA (topological polar surface area) less than or equal to 140 $Å^2$, number of H-bond donors (HBD) less than or equal to 5, MLogP less than or equal to 5, a number of rotatable bonds (nRot) less than or equal to 10 and number of H-bond acceptors (HBA) less than or equal to 10. Furthermore, HL demonstrates favourable physico-chemical properties with a log $P_{o/w}$ (iLOGP) value of 2.74 and a solubility log S (ESOL) value of -7.06. The computed synthetic accessibility score of 2.85 falls within the excellent range, indicating that the compound is highly accessible for synthesis. The ADMET evaluation demonstrates that the newly designed compound HL exhibits high gastrointestinal (GI) absorption and has the potential to inhibit cytochrome enzymes (CYP2C19 and CYP1A2). The remaining physico-chemical parameters are listed in Table-2.

Docking studies: Table-3 provides the computed values for root mean square (RMS), inhibition constant and binding affinity. Prior studies suggest an RMSD value of around 2 Å is generally associated with the optimal docking pose [35,49]. The binding affinity of the ligand HL with the receptors AChE and BChE was evaluated through the inhibition constant (K_i), which indicates the strength of interactions. The inhibition constants for the HL-AChE and HL-BChE complexes were calcu-

TABLE-2
ADMET RESULTS FOR HL

Physico-chemical properties	
Formula	$C_{28}H_{18}N_2O_2$
MW	414.45 g/mol
Num. heavy atoms	32
Num. arom. heavy atoms	26
Fraction Csp3	0.00
HBA	3
nRot	4
HBD	2
Molar refractivity	130.84
TPSA	61.69 Å^2
Pharmacokinetics	
GI absorption	High
BBB permeant	No
P-gp substrate	Yes
CYP2C9 inhibitor	No
CYP2C19 inhibitor	Yes
CYP1A2 inhibitor	Yes
CYP3A4 inhibitor	No
CYP2D6 inhibitor	No
Log K_p (skin permeation)	-3.97 cm/s
Medicinal chemistry	
PAINS	0 alert
Brenk	1 alerts
Leadlikeness	No
Synthetic accessibility	2.85
Lipophilicity	
Log $P_{o/w}$ (iLOGP)	2.74
Log $P_{o/w}$ (WLOGP)	6.21
Log $P_{o/w}$ (XLOGP3)	6.84
Consensus Log $P_{o/w}$	5.38
Log $P_{o/w}$ (SILICOS-IT)	6.33
Log $P_{o/w}$ (MLOGP)	4.77
Water solubility	
Log S (ESOL)	-7.06
Solubility (mg/mL)	3.64×10^{-05}
Class	Poorly soluble
Log S (Ali)	-7.94
Solubility (mg/mL)	4.71×10^{-06} mg/mL
Class	Poorly soluble
Log S (SILICOS-IT)	-10.20
Solubility (mg/mL)	2.60×10^{-08}
Class	Insoluble
Druglikeness	
Lipinski	Yes
Egan	No
Veber	Yes
Ghose	No
Muegge	No
Bioavailability score	0.55

lated as 1.99×10^{-11} M. and 4.91×10^{-10} M, respectively. These values were derived using the formula $K_i = \exp(\Delta G/RT)$ [41,42] where R is the gas constant (1.9872036×10^{-3} kcal/mol K) and T represents the temperature, usually set to 298.15 K (room temperature) and ΔG corresponds to the binding energy. Fig. 10 shows that TRPA84, TYPA121, TYPA334, TRPA276 and ARGA289 are the active sites of AChE. These residues bind with the ligand HL through hydrogen (H) bonding, van der Waals bonds and π-π interactions. The most preferred docking conformation for HL with AChE demonstrates a binding affinity of -14.6 kcal/mol, while the best docking pose of the HL-BChE complex shows a binding affinity of -12.7 kcal/mol. Fig. 11 illustrates the active sites of BChE as TRPA82, ASPA70, GLYA116, SERA198, PHEA329, TRPA231 and PROA285, which interact with the Schiff base compound (HL) through H-bonding, van der Waals contacts, π-π and π-anion interactions. These docking results suggested its potential application for Alzheimer's disease treatment in the current scenario.

TABLE-3
BINDING AFFINITY AND RMSD VALUES FOR DIFFERENT POSES IN THE 1P0I/BChE AND 1EVE/AChE INHIBITOR OF HL

Mode	AChE-HL			BChE-HL		
	Affinity (kcal/mol)	RMSD l.b.	RMSD u.b.	Affinity (kcal/mol)	RMSD l.b.	RMSD u.b.
1	-14.6	0.000	0.000	-12.7	0.000	0.000
2	14.3	1.044	1.942	-12.1	3.443	6.510
3	-14.1	3.249	8.863	-12.1	2.021	2.896
4	-13.5	2.889	8.466	-11.9	0.776	2.856
5	-13.0	2.357	4.147	-11.3	1.426	3.266
6	-12.5	3.237	9.232	-11.2	2.837	6.019
7	-12.1	3.865	9.592	-11.0	2.719	5.569
8	-11.8	2.270	3.654	-10.8	2.712	5.328
9	-11.6	3.632	9.245	-10.6	2.451	3.818

Conclusion

In this work, a novel Schiff base chemosensor for Cu^{2+} ions with a detection limit of 0.25×10^{-6} M has been designed and accomplished. The stoichiometry ratio and association constant were determined using the Benesi–Hildebrand relation, which came out to be 1:1. The optimum pH range for stable complexation of HL–Cu^{2+} complex was 5-9. The binding of Cu^{2+} ions with chemosensor HL was found to be chemically reversible with Na_2EDTA. Further, this fluorescent chemosensor can be used as a potential candidate for study in various biological environments. The DFT calculations revealed that the energy gap is 3.549 eV, while the hardness (1.774 eV) and energy change (–4.20 eV) suggest that the HL possesses electron transfer capability. Finally, the molecular docking and ADMET examination signify its HL potential as an anti-Alzheimer agent and its drug-like character.

ACKNOWLEDGEMENTS

This work was supported by B.R.A. Bihar University, L.S. College and M.P.S. Science College, Muzaffarpur, India.

CONFLICT OF INTEREST

The authors declare that there is no conflict of interests regarding the publication of this article.

REFERENCES

1. S. Xia, S.-Y. Xiao, Q.-Q. Hong, J.-R. Zou, S. Yang, M.-X. Zhang and H. Zuo, *RSC Adv*, **5**, 5244 (2015); https://doi.org/10.1039/C4RA14177F

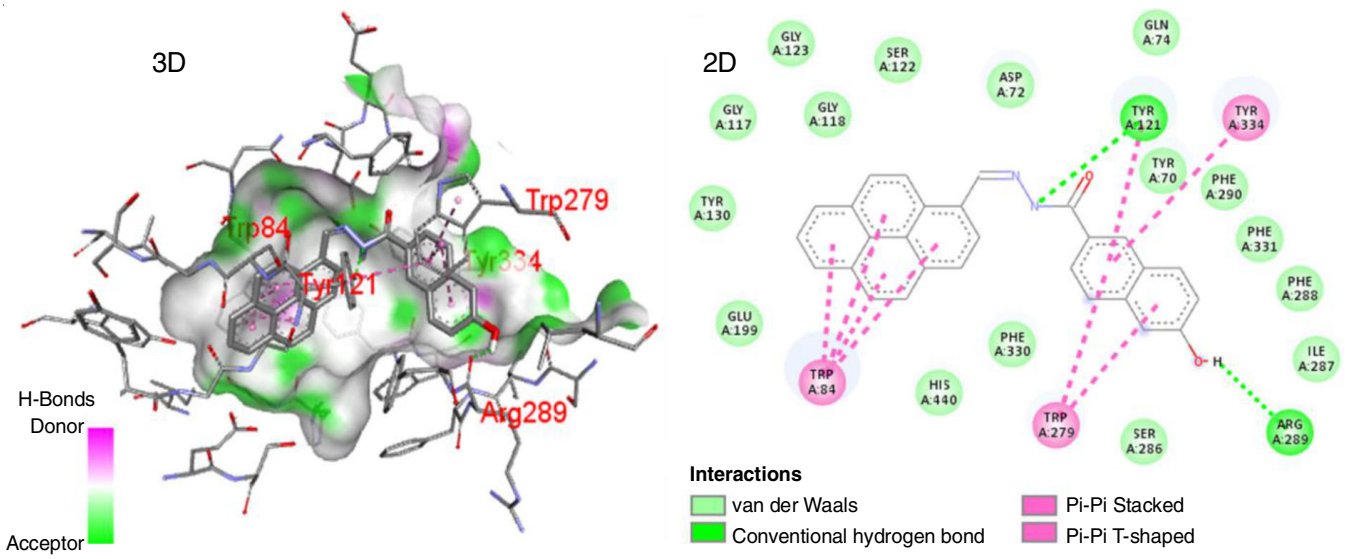

Fig. 10. 3D and 2D docking view for AChE-HL

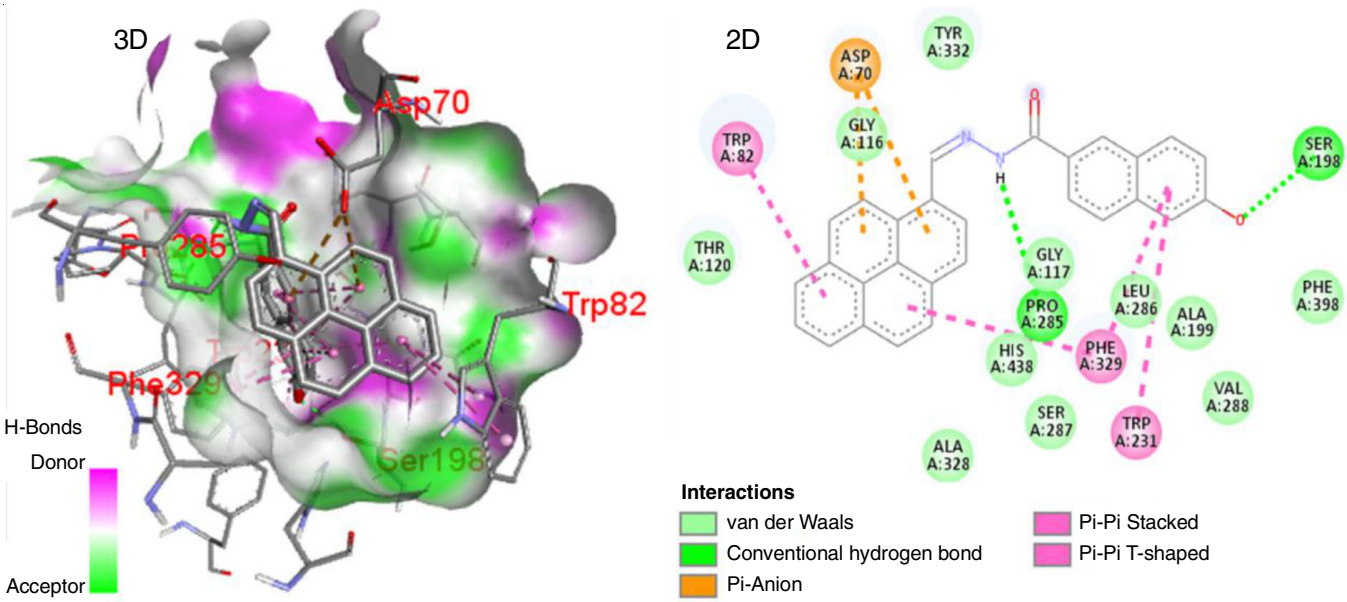

Fig. 11. 3D and 2D docking view for BChE-HL

2. Y. Jeong and J. Yoon, *Inorg. Chim. Acta*, **381**, 2 (2012); https://doi.org/10.1016/j.ica.2011.09.011
3. S. Das, M. Dutta and D. Das, *Anal. Methods*, **5**, 6262 (2013); https://doi.org/10.1039/c3ay40982a
4. M. Formica, V. Fusi, L. Giorgi and M. Micheloni, *Coord. Chem. Rev.*, **256**, 170 (2012); https://doi.org/10.1016/j.ccr.2011.09.010
5. A. Ghosh, A. Sengupta, A. Chattopadhyay and D. Das, *RSC Adv.*, **5**, 24194 (2015); https://doi.org/10.1039/C4RA16768F
6. R. Joseph, B. Ramanujam, A. Acharya and C.P. Rao, *Tetrahedron Lett.*, **50**, 2735 (2009); https://doi.org/10.1016/j.tetlet.2009.03.109
7. X. Xie, X. Chen, B. Li and L. Zhang, *Dyes Pigm.*, **98**, 422 (2013); https://doi.org/10.1016/j.dyepig.2013.03.022
8. L. Zhang, Z. Wang, J. Hou, L. Lei, J. Li, J. Bai, H. Huang and Y. Li, *Anal. Methods*, **10**, 2560 (2018); https://doi.org/10.1039/C8AY00614H
9. Y.H. Hung, A.I. Bush and R.A. Cherny, *J. Biol. Inorg. Chem.*, **15**, 61 (2009); https://doi.org/10.1007/s00775-009-0600-y
10. J.C. Lee, H.B. Gray and J.R. Winkler, *J. Am. Chem. Soc.*, **130**, 6898 (2008); https://doi.org/10.1021/ja711415b
11. E. Madsen and J.D. Gitlin, *Annu. Rev. Neurosci.*, **30**, 317 (2007); https://doi.org/10.1146/annurev.neuro.30.051606.094232
12. J.S. Valentine and P.J. Hart, *Proc. Natl. Acad. Sci. USA*, **100**, 3617 (2003); https://doi.org/10.1073/pnas.0730423100
13. B. Bansod, T. Kumar, R. Thakur, S. Rana and I. Singh, *Biosens. Bioelectron.*, **94**, 443 (2017); https://doi.org/10.1016/j.bios.2017.03.031
14. B. Feier, D. Floner, C. Cristea, E. Bodoki, R. Sandulescu and F. Geneste, *Talanta*, **98**, 152 (2012); https://doi.org/10.1016/j.talanta.2012.06.063
15. T. Gong, J. Liu, X. Liu, J. Liu, J. Xiang and Y. Wu, *Food Chem.*, **213**, 306 (2016); https://doi.org/10.1016/j.foodchem.2016.06.091
16. J. Liu, M. Yu, X.-C. Wang and Z. Zhang, *Spectrochim. Acta A Mol. Biomol. Spectrosc.*, **93**, 245 (2012); https://doi.org/10.1016/j.saa.2012.03.021
17. X. Zhou, S. Lee, Z. Xu and J. Yoon, *Chem. Rev.*, **115**, 7944 (2015); https://doi.org/10.1021/cr500567r

18. S. Yagi, S. Nakamura, D. Watanabe and H. Nakazumi, *Dyes Pigm.*, **80**, 98 (2009); https://doi.org/10.1016/j.dyepig.2008.05.012
19. J.J. Lee, Y.W. Choi, G.R. You, S.Y. Lee and C. Kim, *Dalton Trans.*, **44**, 13305 (2015); https://doi.org/10.1039/C5DT00957J
20. A. Chowdhury, P. Howlader and P.S. Mukherjee, *Chem. Eur. J.*, **22**, 1424 (2016); https://doi.org/10.1002/chem.201504003
21. X. Yue, Z. Wang, C. Li and Z. Yang, *Tetrahedron Lett.*, **58**, 4532 (2017); https://doi.org/10.1016/j.tetlet.2017.10.044
22. M. Sun, L. Du, H. Yu, K. Zhang, Y. Liu and S. Wang, *Talanta*, **162**, 180 (2017); https://doi.org/10.1016/j.talanta.2016.10.012
23. B.N. Giepmans, S.R. Adams, M.H. Ellisman and R.Y. Tsien, *Science*, **312**, 217 (2006); https://doi.org/10.1126/science.1124618
24. Z. Liu, H. Xu, S. Chen, L. Sheng, H. Zhang, F. Hao, P. Su and W. Wang, *Spectrochim. Acta A Mol. Biomol. Spectrosc.*, **149**, 83 (2015); https://doi.org/10.1016/j.saa.2015.04.030
25. S. Comby, S.A. Tuck, L.K. Truman, O. Kotova and T. Gunnlaugsson, *Inorg. Chem.*, **51**, 10158 (2012); https://doi.org/10.1021/ic300697w
26. A.B. Aletti, D.M. Gillen and T. Gunnlaugsson, *Coord. Chem. Rev.*, **354**, 98 (2018); https://doi.org/10.1016/j.ccr.2017.06.020
27. T. Gunnlaugsson, B. Bichell and C. Nolan, *Tetrahedron Lett.*, **43**, 4989 (2002); https://doi.org/10.1016/S0040-4039(02)00895-X
28. D. Wu, A.C. Sedgwick, T. Gunnlaugsson, E.U. Akkaya, J. Yoon and T.D. James, *Chem. Soc. Rev.*, **46**, 7105 (2017); https://doi.org/10.1039/C7CS00240H
29. L. Tang, F. Li, M. Liu and R. Nandhakumar, *Spectrochim. Acta A Mol. Biomol. Spectrosc.*, **78**, 1168 (2011); https://doi.org/10.1016/j.saa.2010.12.072
30. N. Narayanaswamy and T. Govindaraju, *Sens. Actuators B Chem.*, **161**, 304 (2012); https://doi.org/10.1016/j.snb.2011.10.036
31. N. Shao, J.Y. Jin, H. Wang, Y. Zhang, R.H. Yang and W.H. Chan, *Anal. Chem.*, **80**, 3466 (2008); https://doi.org/10.1021/ac800072y
32. H. Zhou, J. Wang, Y. Chen, W. Xi, Z. Zheng, D. Xu, Y. Cao, G. Liu, W. Zhu, J. Wu and Y. Tian, *Dyes Pigm.*, **98**, 1 (2013); https://doi.org/10.1016/j.dyepig.2013.01.018
33. A. Jamal, H. Ferjani, M.S. Haque Faizi and A.Y. Abdullah Alzahrani, *J. Indian Chem. Soc.*, **101**, 101181 (2024); https://doi.org/10.1016/j.jics.2024.101181
34. D. Tatlidil, M.A. Raza, N. Dege, A.A. Agar, U. Farwa and S.U. Rehman, *ACS Omega*, **7**, 10568 (2022); https://doi.org/10.1021/acsomega.2c00102
35. A. Jamal, M.S.H. Faizi and H. Ferjani, *J. Mol. Struct.*, **1319**, 139540 (2025); https://doi.org/10.1016/j.molstruc.2024.139540
36. M.A. Raza and K. Fatima, *J. Phys. Org. Chem.*, **33**, e4076 (2020); https://doi.org/10.1002/poc.4076
37. M.J. Frisch, G.W. Trucks, H.B. Schlegel, G.E. Scuseria, M.A. Robb, J.R. Cheeseman, G. Scalmani, V. Barone, B. Mennucci, G.A. Petersson, H. Nakatsuji, M. Caricato, X. Li, H.P. Hratchian, A.F. Izmaylov, J. Bloino, G. Zheng, J.L. Sonnenberg, M. Hada, M. Ehara, K. Toyota, R. Fukuda, J. Hasegawa, M. Ishida, T. Nakajima, Y. Honda, O. Kitao, H. Nakai, T. Vreven, J.A. Montgomery Jr., J.E. Peralta, F. Ogliaro, M. Bearpark, J.J. Heyd, E. Brothers, K.N. Kudin, V.N. Staroverov, R. Kobayashi, J. Normand, K. Raghavachari, A. Rendell, J.C. Burant, S.S. Iyengar, J. Tomasi, M. Cossi, N. Rega, J.M. Millam, M. Klene, J.E. Knox, J.B. Cross, R.L. Martin, V. Bakken, J.A. Jaramillo, R. Gomperts, R.E. Stratmann, O. Yazyev, R. Cammi, C. Pomelli, J.W. Ochterski, A.J. Austin, K. Morokuma, V.G. Zakrzewski, G.A. Voth, P. Salvador, J.J. Dannenberg, S. Dapprich, A.D. Daniels, Ö. Farkas, J.B. Foresman, J.V. Ortiz, J. Cioslowski and D.J. Fox, Gaussian 09, Revision D.01 Gaussian, Inc., Wallingford CT (2013).
38. O. Trott and A.J. Olson, *J. Comput. Chem.*, **31**, 455 (2010); https://doi.org/10.1002/jcc.21334
39. Z.T. Yilmaz, H.Y. Odabasoglu, P. Senel, V. Adimcilar, T. Erdogan, A.D. Özdemir, A. Gölcü and M. Odabasoglu, *J. Mol. Struct.*, **1205**, 127585 (2020); https://doi.org/10.1016/j.molstruc.2019.127585
40. T. Erdogan, *J. Mol. Struct.*, **1242**, 130733 (2021); https://doi.org/10.1016/j.molstruc.2021.130733
41. S. Ahmed, I. Irshad, S. Nazir, S. Naz, M.A. Asghar, S.M. Alshehri, S. Bullo and M.L. Sanyang, *Sci. Rep.*, **13**, 39496 (2023); https://doi.org/10.1038/s41598-023-39496-6
42. S. Murugavel, S. Sundramoorthy, D. Lakshmanan, R. Subashini and P. Pavan Kumar, *J. Mol. Struct.*, **1131**, 51 (2017); https://doi.org/10.1016/j.molstruc.2016.11.035
43. A. Jamal, M.S.H. Faizi and N. Dege, *J. Mol. Struct.*, **1300**, 137251 (2024); https://doi.org/10.1016/j.molstruc.2023.137251
44. N.M. O'Boyle, A.L. Tenderholt and K.M. Langner, *J. Comput. Chem.*, **29**, 839 (2008); https://doi.org/10.1002/jcc.20823
45. M. Karabacak, L. Sinha, O. Prasad, A.M. Asiri and M. Cinar, *Spectrochim. Acta A Mol. Biomol. Spectrosc.*, **115**, 753 (2013); https://doi.org/10.1016/j.saa.2013.06.092
46. M. Kurban, T.R. Sertbakan and I. Muz, *Mater. Today Commun.*, **39**, 108642 (2024); https://doi.org/10.1016/j.mtcomm.2024.108642
47. M. Ríos-Gutiérrez, A. Saz Sousa and L.R. Domingo, *J. Phys. Org. Chem.*, **36**, e4503 (2023); https://doi.org/10.1002/poc.4503
48. R.G. Parr, L.V. Szentpály and S. Liu, *J. Am. Chem. Soc.*, **121**, 1922 (1999); https://doi.org/10.1021/ja983494x
49. J.-L. Stigliani, V. Bernardes-Génisson, J. Bernadou and G. Pratviel, *Org. Biomol. Chem.*, **10**, 6341 (2012); https://doi.org/10.1039/c2ob25602a